

1 **Simulating the transportation and dispersal of volcanic**
2 **ash cloud with initial condition created by 3D plume**
3 **model**

4 **Key Points:**

- 5 • Creating initial conditions for volcanic ash transport and dispersal models based
6 on 3D plume model output eliminates the need for assumptions or inversion re-
7 garding initial ash particle distribution with height, and improves prediction ca-
8 pability.
9 • Initial particle distribution in vertical direction has greater impact on transport
10 of ash clouds than does horizontal distribution.
11 • Ash particles involved in long-range transport are initially concentrated in the um-
12 brella cloud of large eruptions.

13 **Abstract**

14 VATDs (volcanic ash transportation and dispersion) model atmospheric transport of ash
 15 starting from a source originating at the volcano represented by concentrations of ash
 16 with height. Most VATD models use a source of some prescribed shape calibrated against
 17 an empirical expression for the height-mass eruption rate (MER) relation. The actual
 18 vertical ash distributions in volcanic plume usually vary from case to case and have com-
 19 plex dependencies on eruption source parameters and atmospheric conditions. We present
 20 here for the first time the use of 3D (three-dimensional) plume models to represent ash
 21 cloud sources without any assumption regarding plume geometry. By eliminating assumed
 22 behavior associated with the semiempirical plume geometry, the predictive skill of VATD
 23 simulations are greatly improved. To date no VATD simulation adopts the initial con-
 24 dition created from first principles based 3D plume simulation. We use our recently de-
 25 veloped volcanic plume model based on a 3D Lagrangian method [Cao et al, Geophys-
 26 ical Model Dev., 2018] and couple the output to a standard Lagrangian VATD model
 27 and apply to historical eruptions to illustrate the effectiveness of this approach. The im-
 28 portance of the source model is shown in sensitivity analyses which prove that volcanic
 29 ash transportation simulation is much more sensitive to the source geometry than all other
 30 input parameters. Further investigation also reveals that initial particle distribution in
 31 vertical direction has more impact on transportation of ash clouds than horizontal dis-
 32 tribution. Comparison also indicates that ash particles are concentrated along the in-
 33 trusion height of umbrella cloud that is much lower than the plume top, which is just
 34 momentum overshoot.

35 **1 Introduction**

36 **1.1 Volcanic Ash Transportation Forecast**

37 The fine-grain fraction of tephra (volcanic ash) can be widely dispersed, and can
 38 lead to a degradation of air quality and pose threats to aviation (Tupper et al., 2007).
 39 Identification of volcanic ash helps schedule flights to avoid areas where ash is present.
 40 Numerical estimation of ash distribution using known and forecast wind fields is neces-
 41 sary if we are to accurately predict ash cloud evolution. Numerous VATD (volcanic ash
 42 transportation and dispersion) models have been developed by both civil and military
 43 aviation or meteorological agencies to provide forecasts of ash cloud motion (Witham
 44 et al., 2007). New techniques have been integrated with VATDs to satisfy increasing de-
 45 mands for more outputs, model accuracy and forecast reliability. This contribution ex-
 46 plores a method for creating initial conditions for VATD simulations, which promises to
 47 improve prediction capability and accuracy.

48 ? and Stohl et al. (2011) showed that initial source conditions have significant ef-
 49 ffects on simulation of volcanic ash transportation. Traditional VATD simulation requires
 50 key global descriptors of the volcanic plumes, especially plume height, grain size, erup-
 51 tion duration and mass loading, or alternatively, a mass eruption rate (MER). No mat-
 52 ter how these global descriptors are obtained, they are used to furnish the initial con-
 53 ditions for VATDs in the form of a line-source term of a spatio-temporal distribution of
 54 particle mass. It is a common practice to pick values for these global descriptors using
 55 an empirical expression for the height-MER relation. The empirical expression is writ-
 56 ten as a function of several parameters, including the key global descriptors. The val-
 57 ues for the descriptors can also be found by parameter calibration (e.g. ??Stohl et al.,
 58 2011; Zidikheri et al., 2017). 1D plume models serve as an alternative option to provide
 59 values. For example, ? and “stefanescu2014temporal” (n.d.) used the 1D model puffin
 60 (Bursik, 2001) to generate estimates of mass eruption rate and grain size. In some cases,
 61 an extra step is adopted to spread ash particles from the line source horizontally, result-
 62 ing in an initial ash cloud in 3D space. The horizontal spreading depends on an empir-
 63 ical expression. For example, the VATD model Puff spreads particles from the line source

uniformly in the horizontal direction within a given radius using an empirical expression in puffin. Considering the complexities of volcanic eruptions, the actual ash distribution in initial ash clouds should vary from case to case and with time, making it difficult to find one general expression that is suitable for all cases. It is useful therefore to investigate alternative ways for creating initial ash clouds without assumptions regarding plume geometry or numerical inversion. This provides the major motivation of this paper.

1.2 Numerical Tools

VATD models can be categorized into Lagrangian particle tracking and Eulerian advection-diffusion types. Among several available particle tracking models (e.g. Walko et al., 1995; Searcy et al., 1998; Damours, 1998; Draxler & Hess, 1998) and advection-diffusion models (e.g. Bonadonna & Houghton, 2005; Folch et al., 2009; Schwaiger et al., 2012), we adopt a particle tracking model, Puff (Tanaka, 1991; Searcy et al., 1998), as the primary VATD model. Puff can take 3D ash clouds as initial conditions, which makes it technically easier to couple with 3D plume models. Puff initializes a discrete number of tracers that represent a sample of the eruption cloud, and calculates transport, turbulent dispersion, and fallout for each representative tracer. A cylinder emanating vertically from the volcano summit to a specified maximum height is the standard approach to provide a simple model of the geometry of a typical ash column. Puff minimally requires horizontal wind field data. The “restart feature” of Puff makes it technically feasible to accommodate the hand-off between a plume simulation and the Puff simulation in terms of time and length scales.

We also use another one of the most widely used models for atmospheric trajectory and dispersion calculations, the Hybrid Single-Particle Lagrangian Integrated Trajectory model (HYSPPLIT) (??), developed by NOAA’s Air Resources Laboratory. HYSPPLIT is able to simulate simple back trajectories to very sophisticated computations of transport, mixing, chemical transformation, and deposition of pollutants and hazardous materials. It is used in this study to better understand simulation results by Puff.

Besides parameter calibration, 1D (one dimensional) plume models have been used to obtain global descriptors of volcanic plumes. 1D plume models (e.g. Woods, 1988; Buršík, 2001; Mastin, 2007; de’Michieli Vitturi et al., 2015; Folch et al., 2016; Pouget et al., 2016) solve the equations of motion in 1D using simplifying assumptions, and hence depend on estimation of certain parameters, especially those related to the entrainment of air, which is evaluated based on two coefficients: a coefficient due to turbulence in the rising buoyant jet, and one due to the crosswind field. Different 1D models adopt different entrainment coefficients based on a specific formulation or calibration against well-documented case studies. The feedback from plume to atmosphere is usually ignored in 1D models. While these 1D models generated well-matched results with 3D models for plumes that are dominated by wind (often called weak plumes) much greater variability is observed for strong plume scenarios (Costa et al., 2016). On the other hand, 3D numerical models for volcanic plumes based on first principles and having few parametrized coefficients (Oberhuber et al., 1998; Neri et al., 2003; Y. J. Suzuki et al., 2005; Cermignara, Esposti Ongaro, & Berselli, 2016; Cao et al., 2018) naturally create a 3D ash cloud, which could serve directly as an initial state of the volcanic material for VATDs. However, there is no VATD simulation using such 3D ash clouds as initial conditions. In this paper, we will carry out VATD simulations using an initial state for the ash cloud based on 3D plume simulations, generated with Plume-SPH (Cao et al., 2018; ?). The implementation techniques described in this paper can be applied for any combination of VATD model and 3D plume model even though our investigation is based on a specific VATD model and plume model.

113 **1.3 Pinatubo Eruption**

114 The 1991 eruption of Pinatubo volcano is used as a case study. Pinatubo erupted
 115 between June 12 and 16, 1991, after weeks of precursory activity. The climactic phase
 116 started on June 15 at 0441 UTC and ended around 1341 UTC (?). The climactic phase
 117 generated voluminous pyroclastic flows, and sent Plinian and co-ignimbrite ash and gas
 118 columns to great altitudes (?). The evolution of the Pinatubo ash and SO_2 clouds was
 119 tracked using visible (?), ultraviolet (Total Ozone Mapping Spectrometer; TOMS) (?)
 120 and infrared sensors, including the Advanced Very High-Resolution Radiometer (AVHRR)
 121 (?). There is also sufficient observational data to estimate the eruption conditions for
 122 the climactic phase of the eruption (Y. Suzuki & Koyaguchi, 2009). The availability of
 123 calibrated eruption conditions and extensive observational data regarding ash clouds trans-
 124 port make the Pinatubo eruption an ideal case study.

125 **2 Setting up Simulations**

126 **2.1 Creation of Initial Ash Cloud**

127 The steps to create an initial ash cloud based on the raw output of Plume-SPH are
 128 shown in Fig. 1. The method proposed consists in generating the initial ash cloud di-
 129 rectly from Plume-SPH, foregoing assumptions and estimates or inverse modeling regard-
 130 ing ash injection height and timing thereof. We use Plume-SPH as an example, noting
 131 that for other 3D plume models, the steps would be similar. Plume-SPH is a two-phase
 132 model based on the Lagrangian smoothed-particle hydrodynamics (SPH) method, in which
 133 the computational domain is discretized by SPH particles. The current version, Plume-
 134 SPH 1.0 (Cao et al., 2018), uses two types of SPH particles: 1) particles of phase 1 to
 135 represent ambient air, and 2) particles of phase 2 to represent erupted material. The ini-
 136 tial ash cloud is created from SPH particles of phase 2.

137 After reaching the maximum rise height and starting to spread horizontally, par-
 138 ticles of phase 2 form an initial umbrella cloud (Fig. 2). The 3D plume simulation is con-
 139 sidered complete once the umbrella cloud begins to form. Parcels that will be transported
 140 by the ambient wind are those above the “corner” region, where mean plume motion is
 141 horizontal rather than vertical.

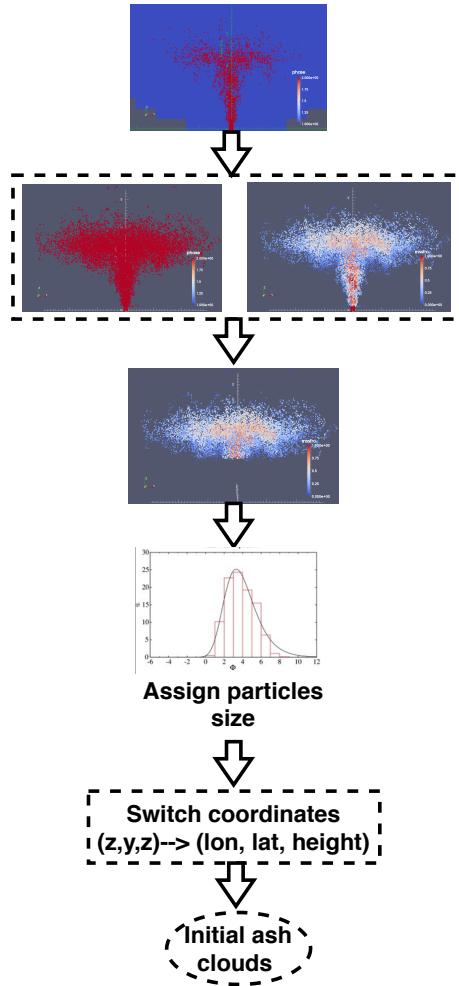
142 Considering that SPH particles are only discretization points, each is assigned a
 143 grain size according to a given total grain size distribution (TGSD) (?), and a concen-
 144 tration according to the mass and volumetric eruption rate. The Plume-SPH discretiza-
 145 tion points are thus switched to Puff Lagrangian tracer particles having grain sizes and
 146 concentrations. The coordinates of these tracer particles, which are initially in the lo-
 147 cal Cartesian coordinate system of Plume-SPH, are converted into Puff’s global coor-
 148 dinate system, which is given in terms of (*longitude, latitude, height*). Puff takes the ini-
 149 tial ash cloud, consisting of the collection of Lagrangian tracer particles with grain size
 150 and concentration, and propagates from time t to time $t+\Delta t$ via an advection/diffusion
 151 equation (Searcy et al., 1998).

152
$$\mathbf{R}_i(t + \Delta t) = \mathbf{R}_i(t) + \mathbf{W}(t)\Delta t + \mathbf{Z}(t)\Delta t + \mathbf{S}_i(t)\Delta t \quad (1)$$

153 Here, $\mathbf{R}_i(t)$ is the position vector of the i^{th} Lagrangian tracer particle at time t , \mathbf{W} ac-
 154 counts for wind advection, \mathbf{Z} accounts for turbulent dispersion and \mathbf{S} is the terminal grav-
 155 itational fallout velocity, which depends on tracer’s size.

156 To summarize, there are four steps to create an initial ash cloud from the raw out-
 157 put of Plume-SPH:

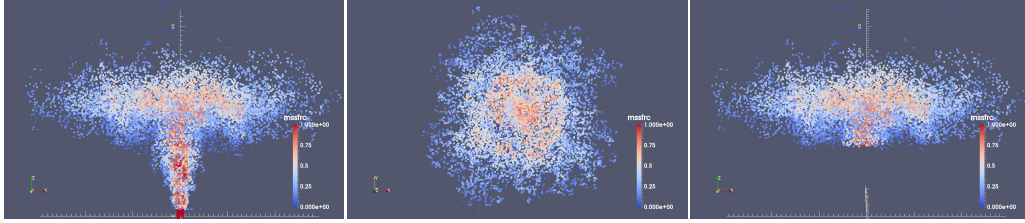
- 158 1. filter by SPH particle type to select SPH particles that represent erupted mate-
 159 rial (phase 2)



127 **Figure 1.** Workflow to create initial condition for Puff based on raw output of Plume-SPH
 128 (Cao et al., 2018). Top: raw output of Plume-SPH. Blue particles are phase 1 (ambient air), red
 129 particles are phase 2 (erupted material). Second row: plume after removing SPH particles of
 130 phase 1. Left: colored according to mass fraction of erupted material. Third row: volcanic plume
 131 above the “corner” region after cutting off the lower portion.

- 165 2. filter by a mean velocity threshold to select the upper part (above the “corner”
 166 region) dominated by horizontal transport
 167 3. switch SPH discretization points to Lagrangian tracer particles, by assigning grain
 168 size to each particle
 169 4. convert coordinates of the SPH Lagrangian tracers into the VATDs’ geographic
 170 coordinate system

171 The features of the volcanic plume and resulting initial ash cloud used in the case study
 172 are shown in Fig. 2. It is important to point out that since both Plume-SPH and Puff
 173 are based on the Lagrangian method, there is no extra step of conversion between an Eu-
 174 lerian grid and Lagrangian particles.



175 **Figure 2.** All particles in the pictures are of type phase 2 (phase 1 has been removed in step
 176 1) at 600s after eruption, at which time, the plume has already reached the maximum height
 177 and started spreading radially. Pictures from left to right are: front view of the whole plume,
 178 top view of the plume and front view of the initial ash cloud, which is essentially a portion of the
 179 whole plume with elevation higher than a given threshold (in this picture is 15000m). Particles
 180 are colored according to mass fraction of erupted material. Red represents high mass fraction
 181 while blue represents low mass fraction.

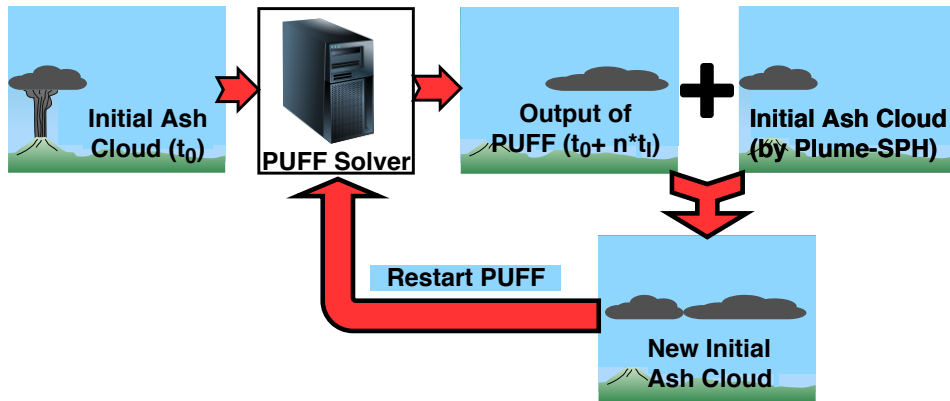
182 Table 1 compares three different methods for creating initial conditions for VATD
 183 simulation: 1) creating initial condition based on parameter calibration without any plume
 184 model (method 1), 2) creating initial condition based on output of 1D plume model (method
 185 2), 3) extracting initial ash cloud from 3D plume simulation (method 3). The first method
 186 determines all global descriptors of volcanic plumes based on calibration. Then create
 187 an initial line source or ash cloud according to semiempirical plume shape expression.
 188 Both other two methods depend on plume models. However 3D plume models can gen-
 189 erate initial ash clouds in 3D space while 1D plume models only obtain global descrip-
 190 tors of plume so still need semiempirical expression to create 3D initial ash clouds. In
 191 addition, the number of Lagrangian tracers is a free parameter when using semiempir-
 192 ical plume shape expressions while it purely depends on simulation when creating ini-
 193 tial conditions from 3D plume simulation results.

196 2.2 Puff Restart

197 The plume and ash transport models are run at different time scales and length
 198 scales. The spatial and temporal resolutions of the plume simulations are much finer than
 199 those of the ash transport model. It takes tens of minutes (600s in this case) for the Pinatubo
 200 plume to reach a steady height. However the eruption persisted for a few hours (9 hours
 201 for the climactic phase of Pinatubo eruption), and it may be necessary to track ash trans-
 202 port for days following an eruption. At present, it is too expensive computationally to
 203 do 3D plume simulations of several hours in real time. In order to handle the difference
 204 in time scale, we mimic a continuing eruption with intermittent pulsed releasing of ash
 205 particles. Particularly, we restart Puff at an interval of 600s, i.e., the physical time of
 206 the plume simulation to reach steady height. At every Puff restart, we integrate the out-

194 **Table 1.** Three different methods for creating initial conditions (initial ash clouds) for Puff
195 simulation

	No model	1D model	3D model
Maximum height	Calibration	Semiempirical	1st principle
Average height	Calibration	Conservation laws (1D)	1st principle
Vertical spread	Calibration	Semiempirical	1st principle
Column radius	Calibration	Conservation laws (1D)	1st principle
Plume shape	Semiempirical	Semiempirical	1st principle
Tracers number	Free parameter	Free Parameter	Based on simulation



216 **Figure 3.** Mimic successive eruption with intermittent pulsed releasing of ash particles. t_l is
217 the period of pulsing release. t_l equals the physical time of 3D plume simulation.

207 put of the last Puff simulation and Plume-SPH into a new ash cloud. This new ash cloud
208 serves as a new initial condition with which to restart a Puff simulation. The interval
209 of the pulsed releases is the simulation time of Plume-SPH, i.e., 600s in our case study.
210 A sketch demonstrating the overall restart process is shown in Fig. (3). The total num-
211 ber of Lagrangian tracer particles used in Puff thus equals the summed number of par-
212 ticles in all releases. So the total number of tracer particles is no longer a user-selected
213 parameter. ? proposed using more realistic time-dependent plume heights. We do not
214 adopt that strategy here for simplicity, although the idea would be straightforward in
215 execution, given time-dependent eruption conditions.

218 2.3 Sensitivity Analysis of Other Parameters

219 Besides the positions of particles in the initial ash cloud, other parameters for Puff
220 simulations are: horizontal diffusivity, vertical diffusivity, mean grain size, grain size stan-
221 dard deviation and total number of tracers. We present in this subsection systematic sen-
222 sitivity studies on these parameters. We also investigate the influence of eruption du-
223 ration. The sensitivity analyses will serve as the basis for identifying possible sources of
224 disparities between simulation and observation.

225 The sensitivity analyses illustrate that adjustment of other parameters produces
226 negligible visual differences in VATD simulation results. Using different vertical diffu-
227 sivities in range of $[100, 100000] m^2 s^{-1}$ and different horizontal diffusivities in range of
228 $[1, 20] m^2 s^{-1}$ produces visually negligible differences. The simulation eruption duration
229 should depend on the total observed duration or the duration of the climactic phase. We
230 conducted several simulations with eruption duration varying in range of $[5, 11] hours$ with

slightly different starting time of climactic phase. Table 2 lists all these simulations. However, only tiny visible differences are observed among the simulated ash transportation. The mean of grain size also has visually ignorable effects on long-term ash transportation according to our sensitivity tests varying the log mean (base 10) grain radius in a range of $[-7.3, -3.5]m$. The standard deviation, when varying in range of $[0.1, 10]$, generates an ignorable difference on long-term ash transportation as well. Similar conclusion on parameter sensitivity is reported by ?Daniele et al. (e.g. 2009). Among these parameters, the eruption duration and beginning time shows, even though tiny, the most obvious influence on simulated ash distribution. In order to show such differences in an intuitive way, Fig. 4 shows simulated ash distribution corresponding to 4.9 hours duration, 9 hours duration and 11 hours duration respectively. After 72 hours, relative to the simulation starting time, these three cases generate generally similar results, with high concentration ash covering almost the same region. The difference of lower concentration distribution is relatively more obvious. Ash cloud covers the broadest area when the eruption duration is 11.1 hours. To summarize, all these parameters have either tiny or ignorable effects on long-term ash distribution simulation.

Table 2. The starting and ending time (UT) for simulating the climactic phase of Pinatubo eruption on June 15 1991. Observed plume height (?) at different time are also listed in the table.

Eruption duration	4.9 hours	9 hours	10 hours	11.1 hours
Start time	0441	0441	0441	0334
Height at start time	37.5 km	37.5 km	37.5 km	24.5 km
End time	0934	1341	1441	1441
Height at end time	35 km	26.5 km	22.5	22.5 km

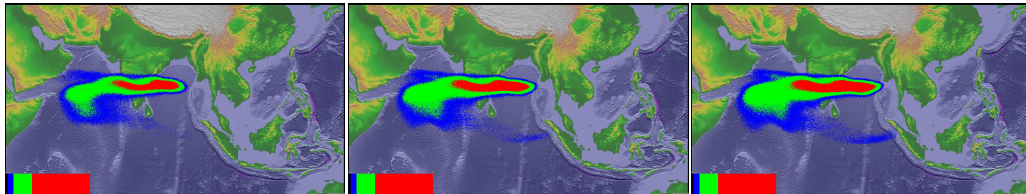
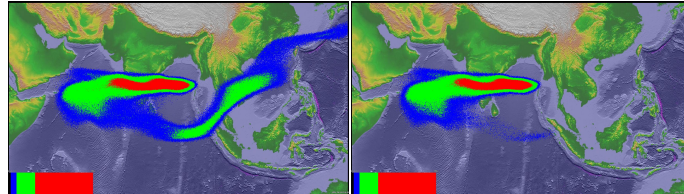


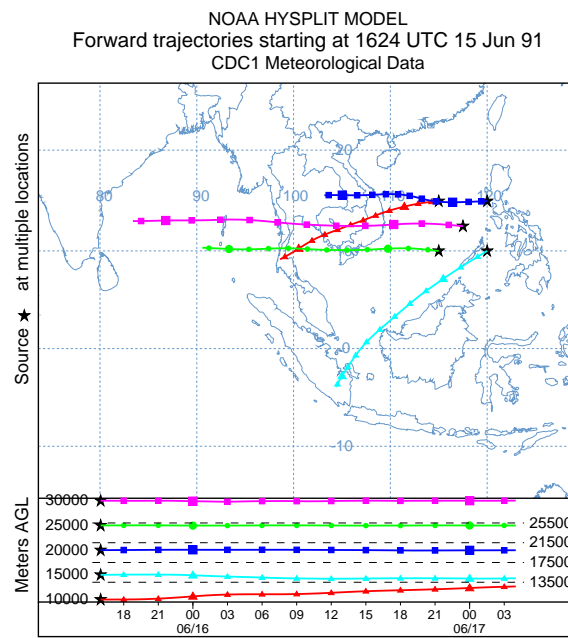
Figure 4. Simulated ash cloud distribution corresponding to eruption duration of 4.9 hours, 9 hours and 11.1 hours (from left to right) respectively. Starting and ending time for each case is in Table 1. The contours are for ash distribution at 72 hours after eruption.

The new methodology for generating initial ash clouds introduces another new parameter: elevation threshold. We also carry out sensitivity analysis on this parameter by varying the elevation threshold from $1500m$ (the height of the vent) to $25000m$. The simulated ash distributions show obviously visible differences. Such influence is especially obvious when the elevation threshold is either very large or very small. However, varying the elevation threshold in the range of $[12000, 18000]m$ generates relatively small differences in ash transportation simulation results. Figure 5 compares the simulated ash distribution corresponding to elevation thresholds of $1500m$ and $15000m$. Compared with ash distribution for threshold of $15000m$, an extra long tail appears when using elevation threshold of $1500m$. Adopting smaller elevation thresholds essentially adds more tracers at lower elevation. As the wind at different elevations are different, these tracers at lower elevation would transpose to different directions. The HYSPLIT (??) forward tra-

265 jectories tracking, which starting at June 15 1624 UTC, indicates that the wind between
 266 evaluation 10000 m to 15000 m blows from north-east to south-west while wind of higher
 267 evaluation blows from east to west (see Fig. 6).



268 **Figure 5.** Simulated ash distribution taking initial ash clouds obtained using different eleva-
 269 tion thresholds (1500m and 15000 m) from output of Plume-SPH. The contours correspond to
 270 ash concentration at 72 hours after eruption. The starting and ending time are corresponding to
 271 9 hours duration case in Table 2



272 **Figure 6.** Trajectories of particles starting from different heights indicating the wind direc-
 273 tions of different evaluations.

The sensitivity analyses demonstrate that the initial condition for VATD simulation has the most significant effect on simulated ash distribution while all other input parameters have either tiny or ignorable influence. The initial ash cloud generated based on semiempirical expression, which is a function of several parameters, might be significantly disparate from a realistic ash cloud. Such initial conditions might greatly compromise the accuracy of VATDs simulation.

In this paper, we do not carry out any investigation with respect to wind field even though it is another dominant factor in VATD simulation. In the case study, we use global *NOAA/OAR/ESRL6 – h, 2.0°* reanalysis wind fields data (???).

3 Comparison and Discussion

Transportation of volcanic ash resulting from the Pinatubo eruption on June 15th 1991 is simulated using two different initial conditions. The first type of initial condition is created in a traditional way according to key global descriptors and semiempirical plume shape expression. The second type of initial condition is created by the new method proposed in this paper. Simulated ash transportation results are compared against observations.

Table 3. List of eruption condition and material properties for plume simulation

Parameters	Units	Plume
Vent velocity	$m \cdot s^{-1}$	275
Vent gas mass fraction		0.05
Vent Temperature	K	1053
Vent height	m	1500
Mass discharge rate	$kg \cdot s^{-1}$	1.5×10^9
Specific heat of gas at constant volume	$J \cdot kg^{-1} \cdot K^{-1}$	717
Specific heat of air at constant volume	$J \cdot kg^{-1} \cdot K^{-1}$	1340
Specific heat of solid	$J \cdot kg^{-1} \cdot K^{-1}$	1100
Specific heat of gas at constant pressure	$J \cdot kg^{-1} \cdot K^{-1}$	1000
Specific heat of air at constant pressure	$J \cdot kg^{-1} \cdot K^{-1}$	1810
Density of air at vent height	$kg \cdot m^{-3}$	1.104
Pressure at vent height	Pa	84363.4

To create initial conditions using the new method described in this paper, the plume rise is simulated first by Plume-SPH. The eruption parameters, material properties and atmosphere for the strong plume no wind case in a comparison study on eruptive column models (Costa et al., 2016) are adopted. Eruption conditions and material properties are listed in Table 3. Note that the density of erupted material at the vent and radius of the vent can be computed from the given parameters. The eruption pressure is assumed to be the same as the pressure of ambient at the vent and hence is not given in the table. The vertical profiles of atmospheric properties were obtained based on the reanalysis data from ECMWF (European Centre for Medium-Range Weather Forecasts) for the period corresponding to the climactic phase of the Pinatubo eruption. The initial ash cloud is obtained by processing the raw output of Plume-SPH following steps described in Sec. 2.

Another set of initial conditions is created based on observed top height (40km) and several other parameters assigned semiempirically (?). These parameters, namely, the global descriptors of volcanic plume, are used as parameters of semiempirical expression to get ash clouds in 3D space. See details in Table 4. Except for initial conditions,

311 the simulation parameters that control VATD simulation are the same for both simu-
 312 lations. As has been shown in the sensitivity analyses section, these parameters have less
 influence on simulation results than initial condition.

303 **Table 4.** Parameters used in VATD simulation of the climactic phase of Pinatubo eruption on
 304 June 15 1991. The first six parameters are used by semiempirical expression to create an initial
 305 ash cloud. When creating an initial condition based on the Plume-SPH model, these parameters
 306 are extracted from output of Plume-SPH model.

Parameters	Unit	Semiempirical	Plume-SPH
Maximum Height (H_{max})	m	40000	41800
Horizontal Spread (R_{max})	km	103.808	-
Vertical Spread (H_{width})	km	6.662	-
Plume Shape	-	Poisson	-
Total Ash Particles	-	1768500	1768500
Elevation Threshold	m	-	15000
Horizontal Diffusivity	m^2/s	10000	10000
Vertical Diffusivity	m^2/s	10	10
Grain Size Distribution	-	Gaussian	Gaussian
Mean of Grain Size (Radius)	mm	3.5×10^{-2}	3.5×10^{-2}
Standard Deviation of Grain Size	-	1.0	1.0
Start Time	UT	0441	0441
End time	UT	1341	1341
Simulation Duration	hour	72	72

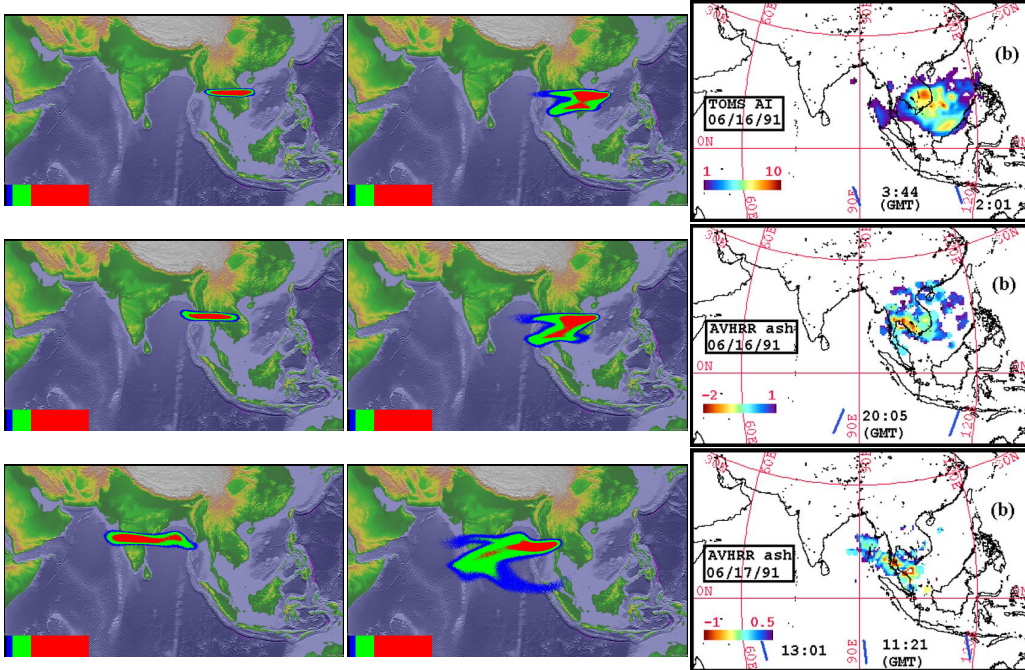
313

314 3.1 “Plume-SPH + Puff” and “Semiempirical Initial Cloud + Puff”

315 The simulation results using different initial conditions are compared with TOMS
 316 images and AVHRR BTD ash cloud map in Fig. 7.

326 The differences between simulated ash transportation by “Semiempirical initial cloud
 327 +Puff” and “Plume-SPH+Puff” are obvious. The simulated ash concentration based on
 328 initial condition created from Plume-SPH is much closer to observation than that based
 329 on semiempirical plume shape expression. Around 23 hours and 31 hours after the be-
 330 ginning of the climactic phase, “Plume-SPH + Puff” simulation generates ash images
 331 that are generally close to observational images, especially the location where high con-
 332 centration ash presents. However, these ash at near west to Pinatubo mountain observed
 333 in satellite images does not show up in “Plume-SPH + Puff” simulation results. This
 334 disparity is very possible due to the fact that the Mountain Pinatubo continued erupt-
 335 ing after the climactic phase while our simulation only simulates the climactic phase. The
 336 ash released after the climatic phase is not accounted for in our simulation results. The
 337 “Semiempirical initial cloud + Puff” simulation, however, forecasts an ash distribution
 338 faster and narrower than observation. The location, where the high concentration ash
 339 presents, is located to the far northwest of observed ash. Around 55 hours after the be-
 340 ginning of the climactic phase, the disparity between observation and simulation becomes
 341 more obvious. Ash distribution of “Semiempirical initial cloud + Puff” simulation lo-
 342 cates far west to the observed ash. The high concentration area of “Plume-SPH + Puff”
 343 simulation, even though closer to observation than that of “Semiempirical initial cloud
 344 +Puff”, is still faster than observation.

345 Except for the initial condition, both simulations adopt the same parameters and
 346 wind field data. That is to say, the only difference between these two simulations is the



317 **Figure 7.** Comparison between “Semiempirical initial cloud + Puff” and “Plume-SPH +
 318 Puff”. Pictures from left to right are: Puff simulation based on initial condition created according
 319 to semiempirical plume shape expression, Puff simulation based on initial condition generated by
 320 Plume-SPH, TOMS or AVHRR image of Pinatubo ash cloud. Ash clouds at different hours after
 321 eruption are on different rows. From top to bottom, the images are corresponding to around 23
 322 hours after eruption (UT 199106160341), 31 hours after eruption (UT 199106161141), 55 hours
 323 after eruption (UT 199106171141). The observation data on the first row are TOMS ash and ice
 324 map. The observation data on the second and third row are AVHRR BTD ash cloud map with
 325 atmospheric correction method applied (?).

347 initial condition. Recall that the initial condition has the most significant influence on
 348 ash transportation simulation. It is therefore very likely that the big difference between
 349 simulation results by “Plume-SPH+Puff” and “Semiempirical initial cloud +Puff” may
 350 be attributed to the initial condition and thereby be credited with its added skill.

351 3.2 Discussion Regarding Maximum Height (H_{max})

352 In this section, we mainly discuss the vertical distribution of ash particles in the
 353 initial ash cloud. The majority of volcanic ash particles usually present a lower eleva-
 354 tion than maximum height. For instance, ?? reported the maximum Pinatubo plume
 355 height as high as around 39km while the cloud heights were estimated at 20 ~ 25km,
 356 ? report the maximum plume height could be > 35km and the plume heights are 23 ~
 357 28km after 15 ~ 16 hours. The neutral buoyant regions of the Pinatubo aerosol esti-
 358 mated by different measurements are: 17 ~ 26km (lidar) by ?, 20 ~ 23km (balloon)
 359 by ?, 17 ~ 28km (lidar) by Jäger (1992), and 17 ~ 25km (lidar) by Avdyushin et al.
 360 (1993). Based on comparison between simulated clouds with early infrared satellite im-
 361 ages of Pinatubo, ? reported that the majority of ash was transported between 16km
 362 and 18km. This is physically understandable as particles are concentrated along the in-
 363 trusion height of the umbrella cloud, not near the top because the plume top is due to
 364 momentum overshoot. However, the empirical expressions for the height-MER relation,

365 which are commonly adopted to create initial conditions for VATD simulation, tend to
 366 place the majority of ash particles closer to top if use observed maximum height in the
 367 empirical expressions.

368 Here we check two commonly used plume shapes, the Poisson and Suzuki. For Pois-
 369 son plume shape, the vertical height of ash particles are determined according to Eq. (2).

$$H = H_{max} - 0.5H_{width} * P + H_{width}R \quad (2)$$

370 where P is an integral value drawn from a Poisson distribution of unit mean, R is a uni-
 371 formly distributed random number between 0 and 1, H_{max} is the maximum plume height,
 372 H_{width} represents an approximate vertical range over which the ash will be distributed.
 373 For Suzuki plume shape (T. Suzuki et al., 1983), volcano ash mass vertical distribution
 374 is assumed to follow the Suzuki equation (Eq. (3)).

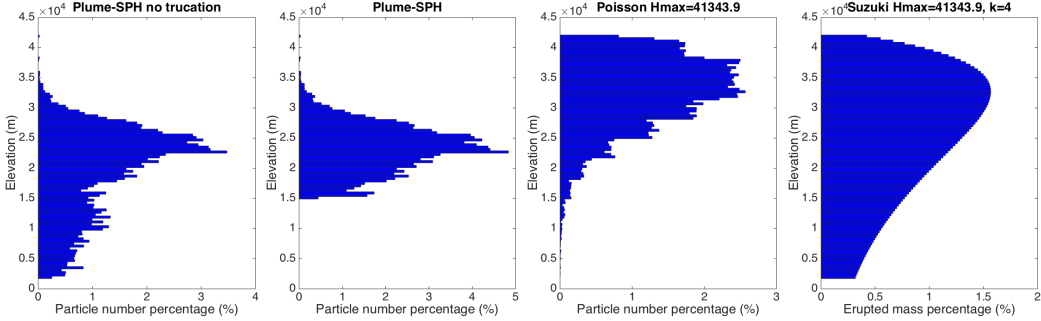
$$Q(z) = Q_m * \frac{k^2(1 - z/H_{max})\exp(k(z/H_{max} - 1))}{H_{max}[1 - (1 + k)\exp(-k)]} \quad (3)$$

375 Where Q_m is the total mass of erupted material, k is shape factor, which is an adjustable
 376 constant that controls ash distribution with height. A low value of k gives a roughly uni-
 377 form distribution of mass with elevation, while high values of k concentrate mass near
 378 the plume top.

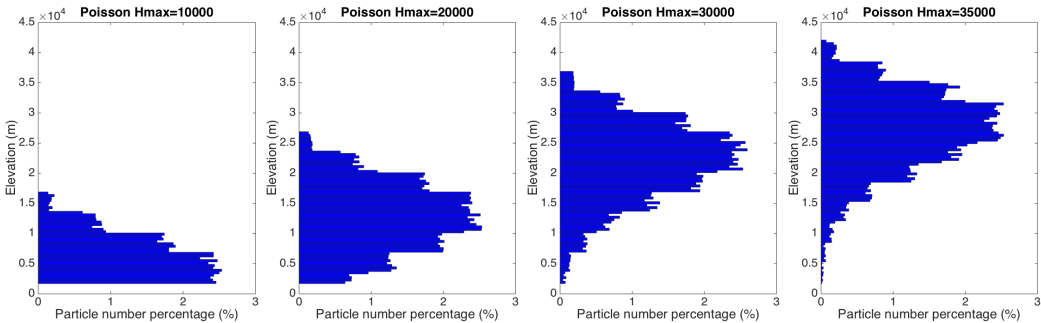
379 Particle distribution (in terms of mass percentage or particle number percentage)
 380 in vertical direction in the initial ash cloud are shown in Fig. 8. In that figure, the ver-
 381 tical particle distribution based on Plume-SPH output is compared with vertical par-
 382 ticle distribution created based on semiempirical shape expressions. Both Poisson and
 383 Suzuki distribution in Fig. 8 take $H_{max} = 40000m$, which is close to reported obser-
 384 vation of maximum height. When adopting Poisson plume shape, the majority of the
 385 particles are between $30km \sim 40km$. Obviously, Poisson distributes majority ash at
 386 a much higher elevation than observations (e.g. ?). As for Suzuki, the majority of ash
 387 particles also distribute in a range that is significantly higher than $25km$. As for initial
 388 ash clouds based on Plume-SPH simulation, the major population of ash particles dis-
 389 tribute between $17km \sim 28km$, which match well with observations. The maximum
 390 height is also consistent with observation. To summarize, using semiempirical plume shape
 391 expression generates an unrealistic initial ash cloud even if we use observed plume max-
 392 imum height.

402 For Poisson and Suzuki plume shape, vertical distribution of ash particles can't be
 403 lower down without changing the maximum height. To distribute a major population
 404 of ash particles at lower elevation, the maximum height has to be reduced to a value smaller
 405 than observed maximum height. Adjusting parameters such as maximum height in the
 406 empirical expression is actually the traditional source term calibration method. A set
 407 of initial ash clouds using different maximum heights based on Poisson plume shape is
 408 shown in Fig. 9). The maximum heights adopted in plume shape expressions are, by no
 409 means, obtained from any plume model or observation. Except for maximum height, all
 410 other parameters for creating an initial ash cloud are the same as these in Table 4. The
 411 range, between which major populations of ash particles locate, is lower when using smaller
 412 maximum heights. These ash clouds created by Poisson distribution with different max-
 413 imum heights are then used as initial conditions in Puff simulation, whose results are shown
 414 in Fig. 10.

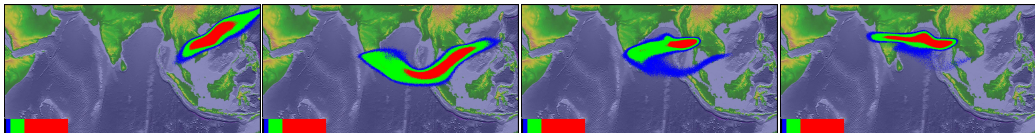
425 Figure 10 shows that the maximum height has significant influence on ash trans-
 426 portation simulation. When the maximum height is $10000m$ the high concentration area
 427 is lag behind observation. While the designated maximum height is $35000m$, the high
 428 concentration area is a little bit faster and much narrower than observation. When us-
 429 ing a maximum height of $41343.9m$, the high concentration area is faster and narrower
 430 than both observation and "Pume-SPH+Puff" simulation results (see Fig. 7). The sim-
 431 ultated high concentration area is closest to "Pume-SPH+Puff" simulation results when



393 **Figure 8.** Particle distribution of initial ash cloud in vertical direction. The picture to the left
 394 is corresponding to the initial ash cloud obtained from Plume-SPH output. The second picture
 395 is corresponding to ash distribution truncated by a elevation threshold of 15000m. The third
 396 picture is for vertical ash distribution based on Poisson distribution with maximum height equals
 397 to 40000m. Another parameter, the vertical spread, in the expression of Poisson plume shape is
 398 6662m. The picture to the right is corresponding to Suzuki distribution with maximum height
 399 equals to 40000m. Another parameter in Suzuki distribution, the shape factor, is 4. The x axis
 400 is the percentage of particle numbers for Plume-SPH and Poisson. For Suzuki the x axis is the
 401 mass percentage of erupted material.



415 **Figure 9.** Initial particle distribution in vertical direction based on Poisson plume shape with
 416 different maximum heights. Pictures from left to right are corresponding to maximum height of
 417 10000m, 20000m, 30000m, 35000m. Another parameter, the vertical spread, in the expression of
 418 Poisson plume shape is 6662m for all cases. The x axis is the percentage of particle numbers. See
 419 Fig. 8 for vertical ash distribution of Plume-SPH output.



420 **Figure 10.** Ash transportation simulated by Puff using different initial ash clouds created
 421 according to Poisson distribution with different maximum heights. Pictures from left to right are
 422 corresponding to maximum plume heights of 10000m, 20000m, 30000m and 35000m. All images
 423 are for simulated ash transportation around 55 hours after eruption (UT 199106171141). See the
 424 observed cloud image in Fig. 7.

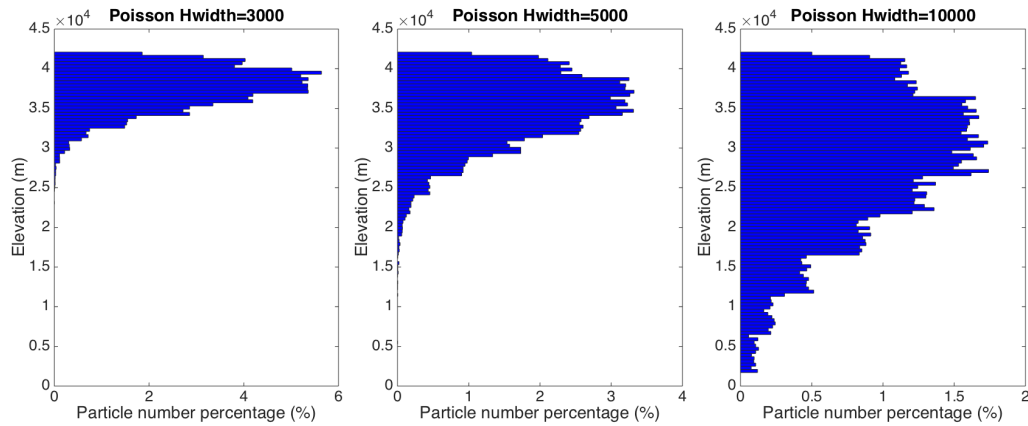
432 assigning a maximum height of 30000m. The front of volcano ash, with lower concen-
 433 tration is faster than observation located far west to high concentration areas. A lower
 434 concentration tailing area also appears in the simulation results while there is no such

tail in the observed image. Puff simulation result based on calibrated maximum height of 30000m shows similar footprint to, even though smaller in terms of covered area than, those of "Pume-SPH+Puff" simulation. However, the initial ash cloud created by Poisson distribution with maximum height around 20000m generates best match ash distribution with observation. That is to say, a maximum height lower than real maximum height is required by Poisson plume shape to distribute ash particles at the same elevation as real ash distribution. This is physically understandable as maximum plume heights are reached due to overshoot. Our hypothesis regarding the sources of disparity between "Semiempirical initial cloud +Puff" simulation and observation is confirmed. Since the initial condition has such a dominant effect on VATD simulation, it is critical for the forecast capability of VATD simulation to explore the more accurate and adaptive ways for establishing the initial conditions, especially the method that does not rely on "post event" parameter calibration.

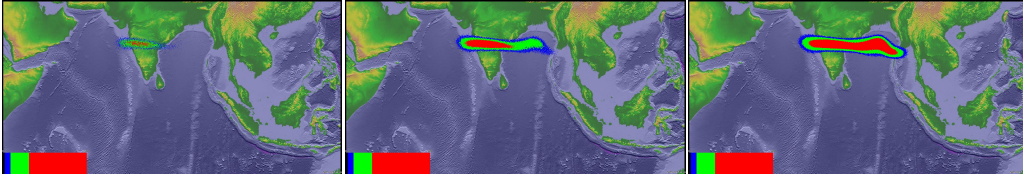
448 3.3 Discussion Regarding Vertical Spread (H_{width})

449 In the previous section, the maximum height is adjusted to change vertical ash distribution along the source line. This section investigates another parameter in semi empirical Poisson expression. We vary the "vertical spread" (H_{width}) in range 3km/ 10km. 450 A set of initial ash clouds created according to different "vertical spread" is shown in Fig. 451 11. Except for "vertical spread", all other parameters for creating an initial ash cloud 452 are the same as these in Table 4. Width of the range within which major populations 453 of ash particles locate become narrower when a smaller value for vertical spread is used. 454 But changing H_{width} has no obvious effect on the height at which the majority of ash 455 particles distribute. These ash clouds based on different vertical spread are then used 456 as initial conditions in Puff simulation, whose results are shown in Fig. 12. 457

458 Adjusting of the vertical spread can change particle distribution in vertical direction 459 and not surprisingly affect VATD simulation results. Unluckily, none of these VATD 460 simulations based on initial ash cloud with vertical spread equals to 3km, 5km, and 10km 461 get better results than VATD simulation based on initial condition created by a 3D plume 462 simulation using Plume-SPH (see Fig. 12). 463



464 **Figure 11.** Vertical particle distribution based on Poisson plume shape with different "ver- 465 tical spread". Pictures from left to right are corresponding to vertical spread of 3km, 5km and 466 10km. The maximum height in the expression of Poisson plume shape is 40000m for all cases. 467 The x axis is the percentage of particle numbers. See Fig. 8 for vertical ash distribution of 468 Plume-SPH output.



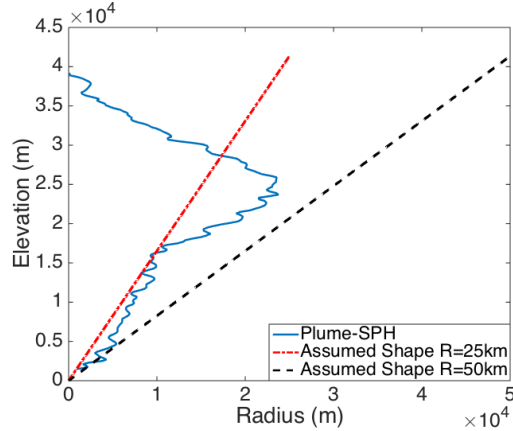
469 **Figure 12.** Ash transportation simulated by Puff using different initial ash clouds created
 470 with different vertical spread. Pictures from left to right are: Puff simulation results based on
 471 initial ash clouds with vertical spread equals to 3000mm, 5000mm and 10000m. The images are
 472 corresponding to around 55 hours after eruption (UT 199106171141). See the observed cloud
 473 image in Fig. 7. The simulated ash field does not adequately cover the observed ash field.

474 The calibrations carried out here are definitely not exhaustive. One might do more
 475 comprehensive calibration throughout the multi-dimensional parameter space (for Pois-
 476 son distribution, the parameter space is two dimensional) and get better matched ash
 477 transportation results. With more complicated plume shape expression, one could have
 478 more control over plume shape and might be able to get an initial condition that is much
 479 closer to the actual initial ash cloud, hence obtaining more accurate ash transportation
 480 prediction. But more complicated plume shape expression usually leads to higher dimen-
 481 sional parameter space which requires more effort to do calibration. Even though, the
 482 degree of freedom to adjust plume shape is still limited. The new method for creating
 483 initial conditions based on 3D plume simulation is more adaptive to various cases and
 484 obviates semi empirical expressions regarding plume shape.

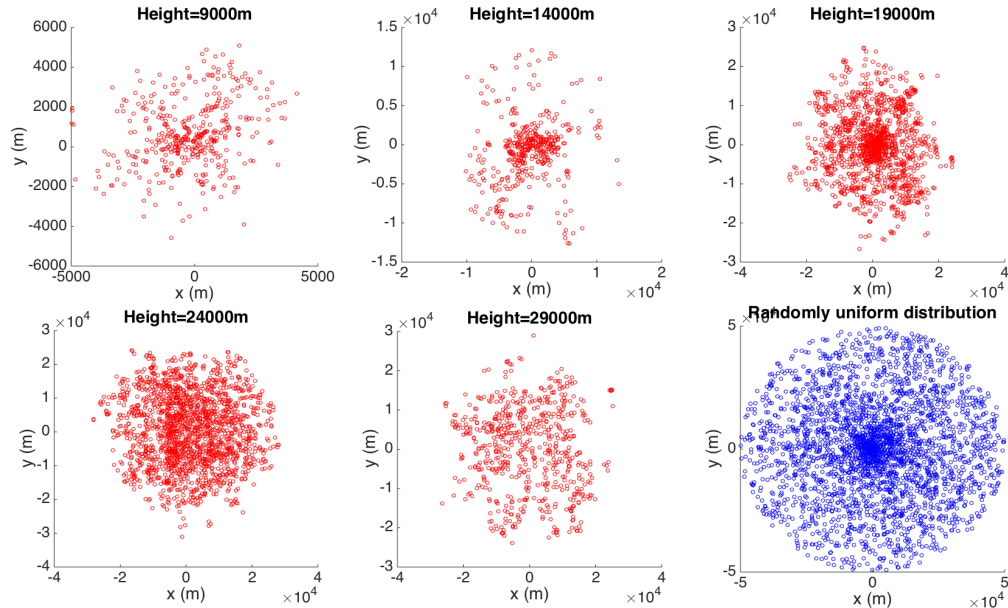
485 3.4 Horizontal Ash Distribution

486 The differences between assumed plume particle distribution and actual (or sim-
 487 ulated by 3D plume) model are not only in vertical direction. Dependence on hori-
 488 zontal particle distribution of the initial ash cloud on ash transportation is investigated in
 489 this section. Puff uses a uniformly distributed random process to determine the ash par-
 490 ticle location in a circle centered on the volcano site. The maximum radius (at top) is
 491 given as “horizontal spread” in Table 4. The horizontal displacement from a vertical line
 492 above the volcano is a random value within a circle of radius, which equals to “horizon-
 493 tal spread” multiplied by the ratio of the particle height H to maximum H_{max} . So the
 494 net shape of the plume is an inverted cone where particles are located directly over the
 495 volcano at the lowest level and extend out further horizontally with increasing plume height.
 496 As for output of Plume-SPH, an effective radius is determined according to a given thresh-
 497 old of ash concentration following Cerminara, Esposti Ongaro, & Neri (2016). A time
 498 averaging and spatial integration of the dynamic 3D flow fields are conducted to get rid
 499 of significant fluctuations in time and space. Fig. 13 compares radius of initial ash clouds
 500 created by 3D plume simulation and assumed plume shape expression adopted in Puff.
 501 Obviously, It is impossible for the simple assumed plume shapes to capture the complex
 502 and more realistic shapes developed by 3D plume simulation of Plume-SPH. Additional
 503 parameterization may generate more reasonable shapes but none are likely to have the
 504 fidelity of the 3D simulation.

510 Comparison between cross-sectional views of the initial ash clouds is shown in Fig.
 511 14. The cross-sectional view of assumed plume shape (last figure in Fig. 14) is similar
 512 to a cross-sectional view of simulated 3D plumes in general sense. However, for simu-
 513 lated 3D plume, the ash particle distribution on cross section varies along with height.
 514 It is hard for semiempirical expressions to have such a distribution. In Puff, particle dis-
 515 tribution on cross sections is assumed to be the same.

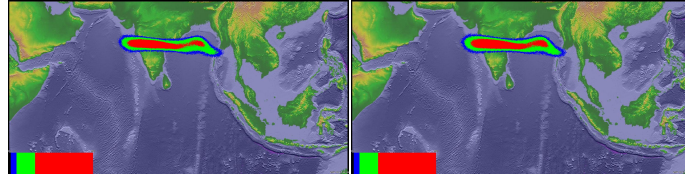


505 **Figure 13.** Comparison between radius of initial ash clouds created by 3D plume model
 506 (Plume-SPH) and assumed initial ash cloud shape in Puff. The plume shape expression used in
 507 Puff defines an inverted cone whose actual shape changes when “horizontal spread” takes differ-
 508 ent values. $R = 25\text{km}$ is corresponding to “horizontal spread” equals to 50km . $R = 50\text{km}$ is
 509 corresponding to “horizontal spread” equals to 100km



516 **Figure 14.** Horizontal distribution of ash particles (tracers) on a cross section of initial ash
 517 cloud. Puff assumes a randomly uniform distribution of ash particles within a circle, as shown
 518 by blue dots in the last figure. All other figures show the ash particle distribution of initial ash
 519 clouds created by Plume-SPH at different elevations.

520 Assigning different values to “horizontal spread” has an ignorable effect on VATD
 521 simulation results. We use numbers between 50km to 1600km as “horizontal spread” to
 522 create initial ash clouds for VATD, all of them generate very similar results. Figure 15
 523 shows two different simulation results based on initial ash clouds with “horizontal spread”
 524 equals to 50km and 600km respectively. No visible differences are apparent between them.
 525 This implies that horizontal distribution has less significant influence on VATD simu-
 526 lation results than vertical distribution.



527 **Figure 15.** Ash transportation simulated by Puff at around 55 hours after eruption (UT
 528 199106171141). Different values for “horizontal spread” are used to create an initial ash cloud.
 529 Pictures to the left are corresponding to “horizontal spread” equals to 50kmm. Pictures to the
 530 right corresponding to “horizontal spread” equals to 600kmm. The observed cloud image is in
 531 Fig. 7.

532 4 Conclusion

533 This paper presented, for the first time, VATD simulations using initial source con-
 534 ditions created by a 3D plume model. Traditional VATD simulations use initial condi-
 535 tions created according to a semiempirical plume shape expression. A case study of the
 536 1991 Pinatubo eruption demonstrates that a 3D plume model can create more realistic
 537 initial ash cloud and ash parcel positions, and therefore improve the accuracy of ash trans-
 538 port forecasts. Informal sensitivity analyses suggest that initial conditions, as expressed
 539 in the disposition of initial ash parcel positions in the vertical, have a more significant
 540 effect on a volcanic ash transport forecast than most other parameters. Comparison of
 541 initial ash parcel distributions among the 3D plume model, semiempirical expressions,
 542 and observations suggests that a major subpopulation of ash parcels should be placed
 543 at a much lower elevation than maximum height to obtain a better VATD forecast. For
 544 the Pinatubo case study, “well-matched” simulation results are observed when using a
 545 maximum height of around 30km, which is much lower than the observed maximum height
 546 of 40km. Comparing the effects of the maximum height, vertical spread and horizontal
 547 spread shows that ash particle distribution in the vertical direction has the strongest ef-
 548 fect on VATD simulation.

549 To summarize, we have presented a novel method for creating *a priori* initial source
 550 conditions for VATD simulations. We have shown that it might be possible to obtain ini-
 551 tial positions of ash parcels with deterministic forward modeling of the volcanic plume,
 552 obviating the need to attempt to obtain initial positions or a history of release heights
 553 via inversion (Stohl et al., 2011). Although the method now suffers from the high com-
 554 putational cost associated with 3D forward modeling, it not only helps overcome short-
 555 comings of existing methods used to generate *a priori* input parameters, but also over-
 556 comes the need to do the thousands of runs associated with inverse modeling. In addi-
 557 tion, computational cost will continue to diminish as computing speed increases. As they
 558 are forward numerical models based on first principles, 3D plume models need little if
 559 any parameterization, and user intervention should not be required to improve forecast
 560 power; no assumption about the initial position of ash parcels is needed. Generation of
 561 the initial cloud of ash parcels directly by 3D simulation is potentially adaptable to a
 562 variety of volcanic and atmospheric scenarios. In contrast, semiempirical expressions used
 563 to determine initial conditions require several parameters to control ash particle distri-
 564 bution along a vertical line source or some simplified shape of the initial ash cloud, mak-
 565 ing it difficult in some cases to generate initial conditions that closely resemble a com-
 566 plex reality.

567 The full range of research issues raised by numerical forecasting of volcanic clouds
 568 is diverse. We described in this paper the effect of initial conditions chosen from the out-
 569 put of a 3D plume model on numerical forecasts of volcanic ash transport simulation.
 570 The wind field, another important factor in volcanic ash transportation simulation is not

571 discussed in the present work. Some other aspects, such as small scale physical processes,
 572 even though they play lesser roles, might need to be included in VATDs to improve ac-
 573 curacy for a particular eruption. In addition, eruption conditions are subject to change
 574 with time, even during the climactic phase of an eruption. In the future, time-dependent
 575 initial conditions for VATDs can be created from 3D plume simulations with time-dependent
 576 eruption conditions.

577 Acknowledgments

578 Support for the Twentieth Century Reanalysis Project dataset is provided by the U.S.
 579 Department of Energy, Office of Science Innovative and Novel Computational Impact
 580 on Theory and Experiment (DOE INCITE) program, and Office of Biological and En-
 581 vironmental Research (BER), and by the National Oceanic and Atmospheric Adminis-
 582 tration Climate Program Office.

583 References

- 584 (n.d.).
- 585 Avdyushin, S., Tulinov, G., Ivanov, M., Kuzmenko, B., Mezhuev, I., Nardi, B., ...
 586 Chanin, M.-L. (1993). 1. spatial and temporal evolution of the optical thick-
 587 ness of the pinatubo aerosol cloud in the northern hemisphere from a network of
 588 ship-borne and stationary lidars. *Geophysical research letters*, 20(18), 1963–1966.
- 589 Bonadonna, C., & Houghton, B. (2005). Total grain-size distribution and volume of
 590 tephra-fall deposits. *Bulletin of Volcanology*, 67(5), 441–456.
- 591 Bursik, M. (2001). Effect of wind on the rise height of volcanic plumes. *Geophys.
 592 Res. Lett.*, 28(18), 3621–3624.
- 593 Cao, Z., Patra, A., Bursik, M., Pitman, E. B., & Jones, M. (2018). Plume-sph 1.0:
 594 a three-dimensional, dusty-gas volcanic plume model based on smoothed particle
 595 hydrodynamics. *Geoscientific Model Development*, 11(7), 2691–2715.
- 596 Cerminara, M., Esposti Ongaro, T., & Berselli, L. (2016). Ashee-1.0: a compressible,
 597 equilibrium-eulerian model for volcanic ash plumes. *Geoscientific Model Develop-
 598 ment*, 9(2), 697–730.
- 599 Cerminara, M., Esposti Ongaro, T., & Neri, A. (2016). Large eddy simulation of
 600 gas-particle kinematic decoupling and turbulent entrainment in volcanic plumes.
 601 *Journal of Volcanology and Geothermal Research*.
- 602 Costa, A., Suzuki, Y., Cerminara, M., Devenish, B., Esposti Ongaro, T., Herzog, M.,
 603 ... others (2016). Results of the eruptive column model inter-comparison study.
 604 *Journal of Volcanology and Geothermal Research*.
- 605 Daniele, P., Lirer, L., Petrosino, P., Spinelli, N., & Peterson, R. (2009). Applications
 606 of the puff model to forecasts of volcanic clouds dispersal from etna and vesuvio.
 607 *Computers & Geosciences*, 35(5), 1035–1049.
- 608 de'Michieli Vitturi, M., Neri, A., & Barsotti, S. (2015). Plume-mom 1.0: A new
 609 integral model of volcanic plumes based on the method of moments. *Geoscientific
 610 Model Development*, 8(8), 2447–2463.
- 611 Draxler, R. R., & Hess, G. (1998). An overview of the hysplit_4 modelling system for
 612 trajectories. *Australian meteorological magazine*, 47(4), 295–308.
- 613 Damours, R. (1998). Modeling the etex plume dispersion with the canadian emer-
 614 gency response model. *Atmospheric Environment*, 32(24), 4335–4341.
- 615 Folch, A., Costa, A., & Macedonio, G. (2009). Fall3d: A computational model for
 616 transport and deposition of volcanic ash. *Computers & Geosciences*, 35(6), 1334–
 617 1342.
- 618 Folch, A., Costa, A., & Macedonio, G. (2016). Fplume-1.0: An integral volcanic
 619 plume model accounting for ash aggregation. *Geoscientific Model Development*,
 620 9(1), 431.

- 621 Jäger, H. (1992). The pinatubo eruption cloud observed by lidar at garmisch-
 622 partenkirchen. *Geophysical research letters*, 19(2), 191–194.
- 623 Mastin, L. G. (2007). A user-friendly one-dimensional model for wet volcanic
 624 plumes. *Geochemistry, Geophysics, Geosystems*, 8(3).
- 625 Neri, A., Esposti Ongaro, T., Macedonio, G., & Gidaspow, D. (2003). Multiparticle
 626 simulation of collapsing volcanic columns and pyroclastic flow. *Journal of Geo-
 627 physical Research: Solid Earth (1978–2012)*, 108(B4).
- 628 Oberhuber, J. M., Herzog, M., Graf, H.-F., & Schwanke, K. (1998). Volcanic plume
 629 simulation on large scales. *Journal of Volcanology and Geothermal Research*,
 630 87(1), 29–53.
- 631 Pouget, S., Bursik, M., Singla, P., & Singh, T. (2016). Sensitivity analysis of a one-
 632 dimensional model of a volcanic plume with particle fallout and collapse behavior.
 633 *Journal of Volcanology and Geothermal Research*.
- 634 Schwaiger, H. F., Denlinger, R. P., & Mastin, L. G. (2012). Ash3d: A finite-volume,
 635 conservative numerical model for ash transport and tephra deposition. *Journal of
 636 Geophysical Research: Solid Earth*, 117(B4).
- 637 Searcy, C., Dean, K., & Stringer, W. (1998). Puff: A volcanic ash tracking and pre-
 638 diction model. *Journal of Volcanology and Geothermal Research*, 80, 1–16.
- 639 Stohl, A., Prata, A., Eckhardt, S., Clarisse, L., Durant, A., Henne, S., ... others
 640 (2011). Determination of time-and height-resolved volcanic ash emissions and
 641 their use for quantitative ash dispersion modeling: the 2010 eyjafjallajökull erup-
 642 tion. *Atmospheric Chemistry and Physics*, 11, 4333–4351.
- 643 Suzuki, T., et al. (1983). A theoretical model for dispersion of tephra. *Arc volcan-
 644 ism: physics and tectonics*, 95, 113.
- 645 Suzuki, Y., & Koyaguchi, T. (2009). A three-dimensional numerical simulation of
 646 spreading umbrella clouds. *Journal of Geophysical Research: Solid Earth (1978–
 647 2012)*, 114(B3).
- 648 Suzuki, Y. J., Koyaguchi, T., Ogawa, M., & Hachisu, I. (2005). A numerical study
 649 of turbulent mixing in eruption clouds using a three-dimensional fluid dynamics
 650 model. *Journal of Geophysical Research: Solid Earth*, 110(B8).
- 651 Tanaka, H. (1991). Development of a prediction scheme for the volcanic ash fall
 652 from redoubt volcano. In *First int'l. symp. on volcanic ash and aviation safety*
 653 (Vol. 58).
- 654 Tupper, A., Itikarai, I., Richards, M., Prata, F., Carn, S., & Rosenfeld, D. (2007).
 655 Facing the challenges of the international airways volcano watch: the 2004/05
 656 eruptions of manam, papua new guinea. *Weather and Forecasting*, 22(1), 175–
 657 191.
- 658 Walko, R., Tremback, C., & Bell, M. (1995). Hypact: The hybrid particle and con-
 659 centration transport model. *Users guide*.
- 660 Witham, C., Hort, M., Potts, R., Servranckx, R., Husson, P., & Bonnardot, F.
 661 (2007). Comparison of vaac atmospheric dispersion models using the 1 november
 662 2004 grimsvötn eruption. *Meteorological Applications*, 14(1), 27–38.
- 663 Woods, A. (1988). The fluid dynamics and thermodynamics of eruption columns.
 664 *Bulletin of Volcanology*, 50(3), 169–193.
- 665 Zidikheri, M. J., Lucas, C., & Potts, R. J. (2017). Estimation of optimal dispersion
 666 model source parameters using satellite detections of volcanic ash. *Journal of Geo-
 667 physical Research: Atmospheres*, 122(15), 8207–8232.